15

Automated system for measuring the surface shape of large flat an cylindrical mirrors using a Fizeau type interferometer

© E.I. Glushkov, I.V. Malyshev, A.I. Nikolaev, E.V. Petrakov, N.I. Chkhalo, R.A. Shaposhnikov

Institute of Physics of Microstructures, Russian Academy of Sciences,
603950 Nizhny Novgorod, Russia
e-mail: eglushkov@ipmras.ru

Received June 25, 2025
Revised June 25, 2025
Accepted June 25, 2025

An automated system for measuring the surface shape of mirrors with dimensions larger than the Fizeau interferometer aperture and cylindrical mirrors using the Fizeau interferometer is described. The system is based on the Zygo Verifire interferometer with an 100 mm aperture. A sample is placed on a motorized translation stage system designed to provide linear motion along the interferometer aperture and tilting about the axes perpendicular to the optical axis of the interferometer, and movements necessary to perform measurements using a subaperture cross-linking technique. Cross-linking is performed at the end of measurements using an overlap matrix technique. The system made it possible to define the systematic measurement error, including the reference surface error, using a unidirectional multi-shifted method, to consider the error during measurements, and perform measurements with a repeatability of 15 pm and subnanometer accuracy.

Keywords: Fizeau interferometer, high-coherence interferometry, subapertures, automated 3*D* system, Kirkpatrick–Baez nanofocusing system.

DOI: 10.61011/TP.2025.10.62089.170-25

Introduction

High precision metrology of substrates and finished mirrors generally involves high-coherence (laser) interferometry techniques. In particular, the Fizeau interferometers are the most widely used systems [1–3]. Interferometers measure the difference between wavefronts reflected from the test surface (test wavefront) and the reference surface (reference wavefront). Consequently, any reference surface errors contribute to the measurement bias. Attainable accuracy of reference surfaces has traditionally limited the employment of the Fizeau interferometers for characterizing X-ray optics that requires high accuracy at large apertures. Therefore, X-ray optics metrology was performed using angle measurement instruments such as LTP (Long Trace Profiler) [4] and NOM (Nanometer Optical Measuring Machine) [5]. Evolvement of subaperture cross-linking measurements has made it possible to measure long flat and cylindrical mirrors using the Fizeau interferometer with a subnanometer accuracy [6–8]. Cross-linking techniques use data redundancy in overlapping regions between adjacent measurements to combine the measured subapetures [9]. The advantage of the Fizeau interferometer is in its ability to measure simultaneously a surface area larger than the area of profilometers.

Consideration of the Fizeau interferometer measurement bias (absolute measurement), in particular, the reference surface error, is necessary for optical surface measurement with an accuracy of several nanometers and better. High precision reference mirrors for the Fizeau interferometer are very expensive and generally have a shape that is less accurate ($\lambda/20$, $\lambda/50$ PV (peak-to-valley) height — 30–10 nm) than that of the high precision planes to be measured (several nm for PV).

Absolute measurement techniques include a liquid plane technique [10], pseudo-shift technique [11], three plane techniques and versions [12]. Measurement of the diffraction grating surface also allows the interferometer path to be calibrated and measurement bias to be determined [13]. A traditional three plane technique is based on relative measurements of three planes using particular polynomial approximations with a predefined maximum degree to provide the absolute shape of the test surface. Disadvantage of the approach is in that it cannot consider shape errors with a spatial frequency higher than the chosen one and singular shape errors. The need for using three expensive reference surfaces is a considerable disadvantage of the tree plane technique. Modern absolute measurement techniques are based on the analysis of data contained in each pixel and do not use polynomial surface approximation, thus providing high spatial resolution of measurements.

The unidirectional multi-shifted method [14,15] is used to determine the Fizeau interferometer measurement bias using only two reflecting (reference and test) flats. A unidirectional multi-shift provides a redundant data set concerning the test surface that allows for composing an overdetermined system of linear equations, solution of which gives information about the measurement bias. Moreover, this approach avoids the effect of high-frequency artefacts on measurements, for example, interference rings induced by test and reference wavefront diffraction on reference surface defects (dust particles) [16].

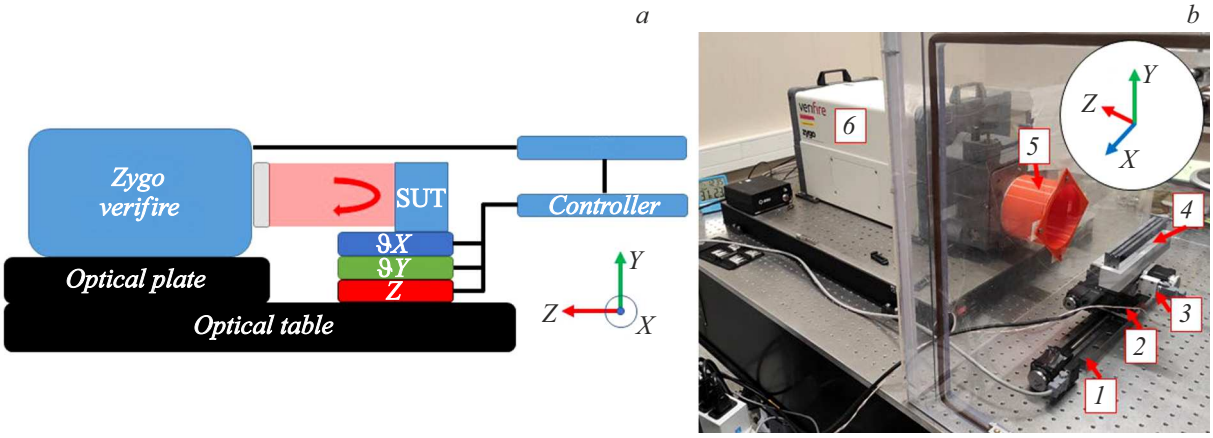

Figure 1. Metrological system for mirror measurement *1* — linear Z translation stage; *2* — ϑY rotation stage; *3* — ϑX rotation stage; *4* — measured surface; *5* — protection screen against ambient air flow that connects the interferometer enclosure and reference surface; *6* — Fizeau interferometer.

Development of our measurement system has been incentivized by the Shared Research Facility „SCPS“ project being implemented in Russia [17], for which the Institute of Physics of Microstructures, Russian Academy of Sciences, has created a double-mirror multilayer monochromator (DMM) [21,22] and Kirkpatrick-Baez (KB) nanofocusing system [18] for station 1-1 „Mikrofokus“ [18–20]. Two flat mirrors 200 mm in length were to be made for DMM. For the KB system, these are two elliptical cylindrical mirrors 200 mm in length.

This work describes a measurement system created by the Institute of Physics of Microstructures, Russian Academy of Sciences, for metrology of large (for the purpose of this work, large means surfaces with dimensions exceeding the interferometer aperture) flat and cylindrical mirrors (mirrors or test surfaces are hereinafter referred to as these two types of mirrors, unless otherwise specified) in an automatic mode. Notwithstanding that the focus is made on the above-mentioned types of mirrors, this system may be used to measure much more types of parts.

1. Measurement system configuration

Figure 1 shows the measurement system created by the Institute of Physics of Microstructures, Russian Academy of Sciences, for high precision measurements of mirror surface shape. The Zygo Verifire interferometer ($\lambda = 632.8$ nm) with a flat reference surface (4″, PV $< \lambda/20$) is used as the Fizeau interferometer. A wavefront reflected from the reference surface is the reference wavefront.

A test surface (TS) is placed on the translation stage system (Standa, Lithuania): linear (8MT160-300) Z translation stage, (8MR151) ϑY rotation stage and (8MG00V-80) ϑX rotation stage. For specifications, see the manufacturer's web site [23]. TS and the translation stage system are placed in an enclosure insulating the system from ambient air flow and dust. The enclosure is additionally connected to the interferometer by a protective screen (Figure 1, *5*). The measurement system is placed on an optical table supported on concrete slabs of the building. Measurements are fully automatic.

ATMega2560, controller and TB6600 stepper motor drivers are used.

2. Analysis of sources of measurement errors

Bias errors (discussed at the end of this work) and random errors affect the surface shape measurement accuracy. Random errors lead to measurement repeatability reduction. For subnanometer accuracy measurements, measurement repeatability shall be better than a nanometer. The main factors affecting measurement repeatability are air flow in the area between the reference and test surfaces, and measurement system vibrations. Measures taken to minimize the effect of these factors are described below.

The main causes of air flow in our measurement room are various items whose temperature differs considerably from room temperature. Such items may include the measurement system operator, interferometer laser, stepper motors, running electrical devices (computers, controllers, power units). Figure 2 shows some local temperatures in the measurement system. Temperature was measured using the A-BF RX-500 thermal imager (resolution 256 × 192 pixels, China).

The following measures were taken to insulate the area between the reference and test surfaces from ambient air flow. First, TS on the translation stage system is placed in the enclosure. Because of the fact that the interferometer warms up to $\sim 40\,^{\circ}$C during operation, it is placed outside the enclosure. Second, a protective screen was made to connect the enclosure and the interferometer reference surface. The gap between the screen and reference surface

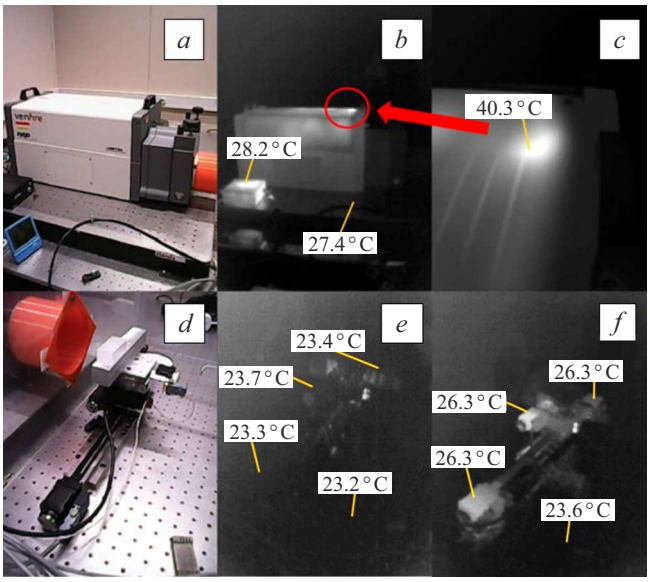

Figure 2. Main heat sources in the measurement system: *a* — visible light image of the interferometer; *b* — IR image of the interferometer that has achieved the operating temperature; *c* — magnified image of the hottest interferometer point enclosed in the red circle in *b*; *d* — visible light image of translation stages; *e* — IR image of translation stages during measurement without a motor holding mode; *f* — image of translation stages with motors set to a holding mode.

is 1 mm, which avoids the influence of the screen on the reference surface shape as experience has shown.

Stepper motors (SM) serve as the main heat source inside the enclosure. To minimize the effect of motor heating on the measurements, the translation stages shall be placed as far as possible so that the motors are outside the area between the reference and test surfaces. The figure shows that the measurement with running motors induces significant surface shape distortions, RMSD of the surface shape increased from 1.4 nm to 2.3 nm.

SMs get warm in two cases. First, when clock pulses are supplied for motor rotation. Second, when holding current is applied. Typical operating modes of the translation stages shall be preliminary described. The linear Z translation stage moves at finite distances where TS is measured. The ϑY and ϑX rotation stages are set to a single-step mode with an interval of at least 1 s between steps. To minimize motor warming, the lowest driver current, at which movement without missing the steps is possible, shall be set in the first case. In the second case, a mode without holding currents was chosen. The following operating current settings are used: ϑX rotation stage — 0.3 A, ϑY rotation stage — 0.5 A, X translation stage — 0.8 A.

Motor temperature measurements of the ϑZ and ϑX translation stages during single-step movements at 1 s intervals have shown that motors don't get warm. Linear translation stage travel continuously during scanning, which causes warming up to a temperature that depends on the SM winding current, resistance and travel time. The linear translation stage motor in our system is at a significant distance from the area between the reference and test surfaces (Figure 1 and 2) and doesn't affect the measurement repeatability.

To minimize the air flow and temperature gradient effect in the area between the reference and test surfaces, the distance between the two surfaces shall be as small as possible. In [24] it is shown that the optimum distance between the reference surface and TS shall be equal to several centimeters to achieve the subnanometer measurement accuracy.

Figure 4 shows repeatability measurements in our system. For clarity, the measured screen effect on repeatability is shown with and without the screen. It can be seen that the screen provides measurement repeatability of 15 pm with respect to RMSD. Such approach to ambient air flow insulation provides high measurement repeatability with small number of averaging. Its disadvantage is in that there are still slow heat fluxes in the system and their effect cannot be effectively minimized by averaging. In [25], the authors demonstrated that addition of random air flow into a measurement system using fans and the optimum number of averaging made it possible to reduce the effect of slow residual fluxes and to reach a repeatability of 1 pm with respect to RMSD.

Vibrations considerably affect the measurements. First, they reduce the measurement repeatability. Second, they induce an interference band imprinting effect when the phase shift method is used to determine the surface shape [26]. Building vibrations and translation stage motors are vibration sources in the measurement room.

To minimize the vibration effect of the building where measurements are performed, the measurement system was assembled on a vibration-insulated optical table installed on the building foundation.

Base resolution (minimum step) of theϑY and ϑX translation stages precludes effective minimization of the tracing error (for details of tracing, see below). Therefore, the translation stages are controlled in a microstepping mode with the 1:16 ratio. This operating mode negatively affects stability of the set rotor position, which results in significant motor vibrations in some positions. To avoid the effect of such vibrations, the motor holding current is released after completion of movement. Note that holding current release after movement doesn't lead to an uncontrolled variation of the motor rotor position during one-way movement.

3. Band zero adjustment method for flat mirrors

The next important factor that shall be considered to increase the measurement accuracy is the ray tracing error [27]. Tracing error for flat mirrors is in the fact that, when the mirror and reference surface are nonparallel, rays reflected from the sample surface travel in the interferometer

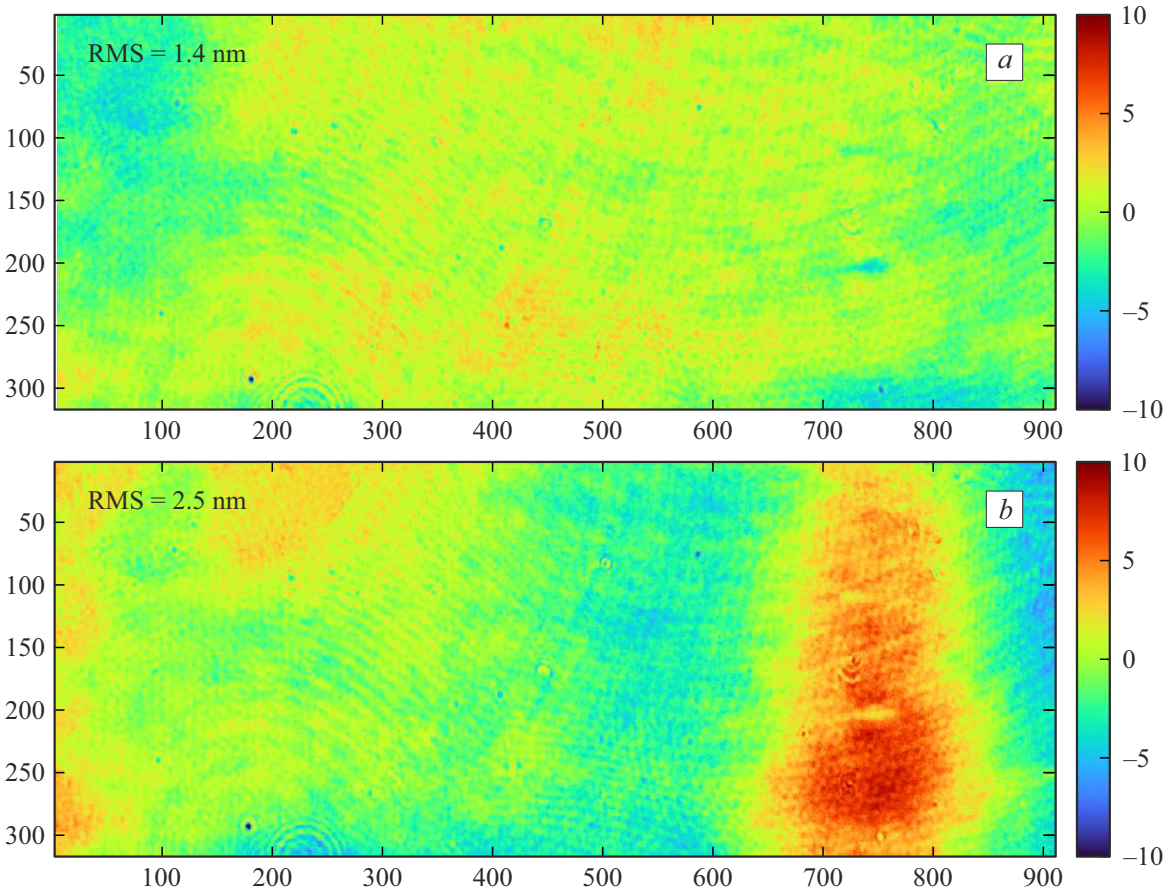

Figure 3. Measurement of the same TS region: *a* — without current in stepper motor windings; *b* — with current in stepper motor windings.

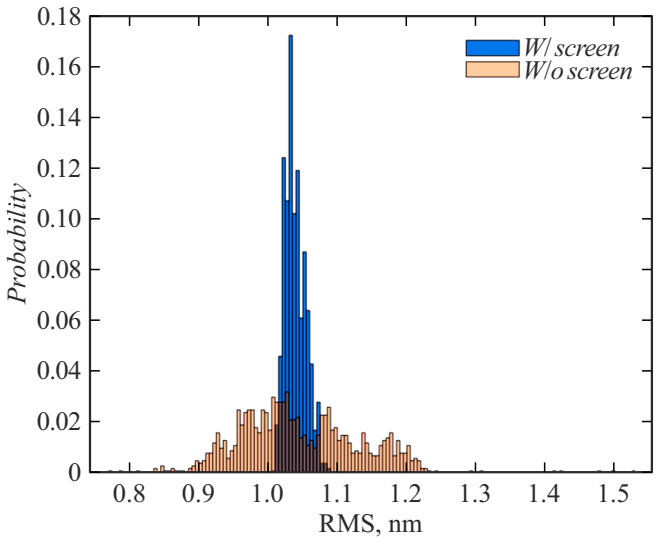

Figure 4. Protective screen effect on the measurement repeatability: $\sigma_{with\ screen} = 15$ pm, $\sigma_{without\ screen} = 90$ pm.

optics along a path other than that travelled by the reference wave. Figure 5 shows the tracing error effect on the measurements. Mirror tilting with respect to the reference surface leads to a significant change in the intensity in some areas of the surface map, and RMSD may vary from 0.97 nm to 1.2 nm.

To minimize the tracing error, a sample movement method was developed to achieve a state with zero interference bands. The method includes the following steps:

1. Binarized image of the interference pattern divides the latter into regions of ones and zeros. Ones correspond to bright bands, and zeros correspond to dark bands. For further reasoning, it is assumed that there are N bright bands;

2. Bright bands are approximated by straight lines $y = k_i x + b_i$, $i = 1 \ldots N$ by the least-square method, whence the mean band angle is derived $\alpha = \Sigma \mathrm{atg}(k_i)/N$;

the 3. ϑX-translation stage is used to achieve the state when $\alpha = 90°$;

the4. ϑY-translation stage is used to achieve $N = 1$;

5. Then, by rotation in the positive and negative directions near $N = 1$, we find a position, at which the mean normalized interference pattern intensity is close to zero or one at a particular threshold, which corresponds to a state with zero interference bands;

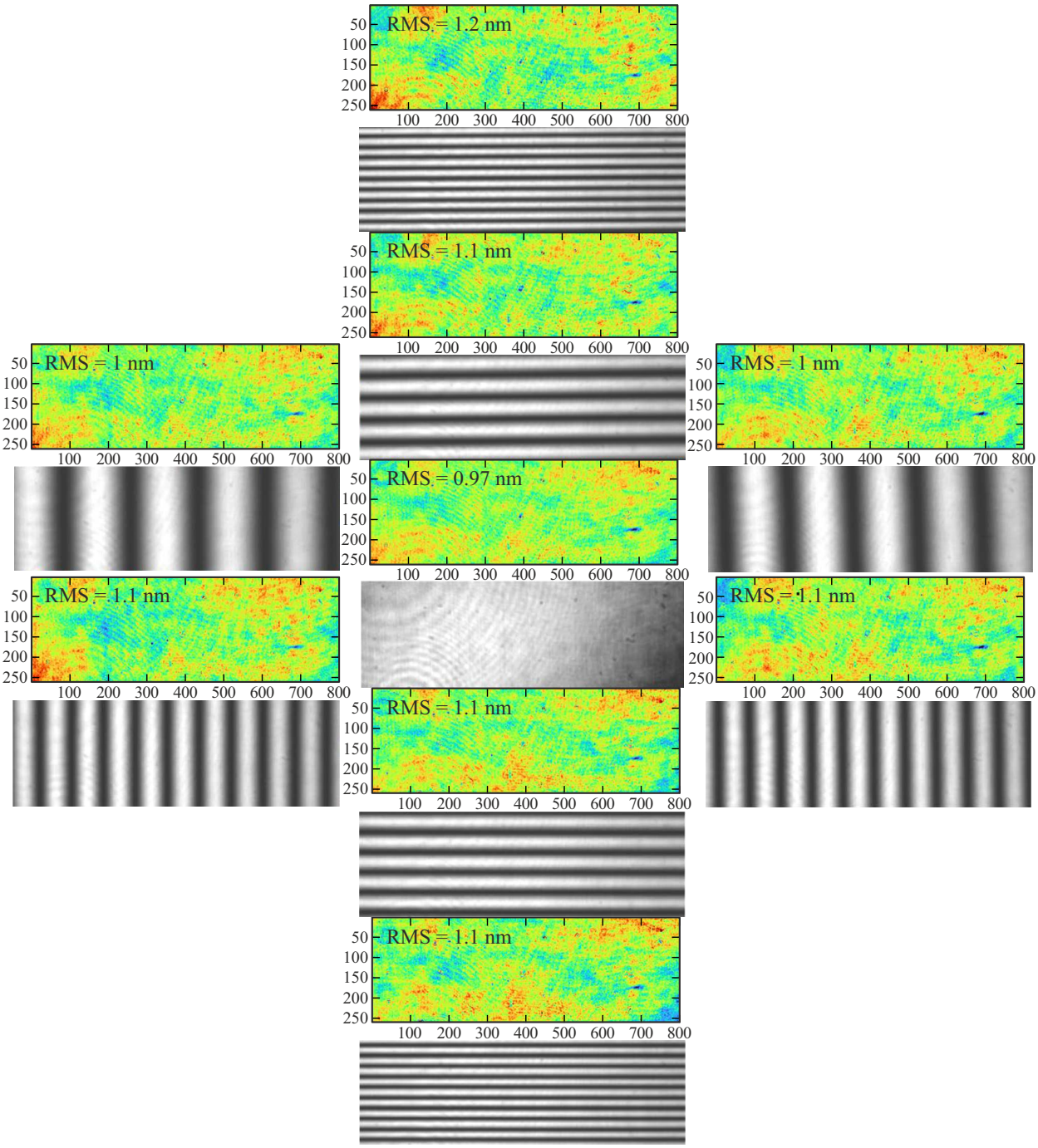

Figure 5. Demonstration of the effect of the number of bands on the measurement result.

6. Wait for 10 s (Zygo Verifire software uses an interference pattern to determine relative vibrations of the reference wavefront and a wavefront reflected from the test surface using the Environment Test function. Using this function, it can be seen that intense vibrations occur at frequencies near 0.15 Hz after the linear movement. Vibration RMSD exceeds 1 nm. Assuming that for decay of the most intense vibration at the lowest frequency, the vibration shall make at least 1 period, the delay time was set to 10 s. Observations show that this approach provides measurements with vibration RMSD lower than 1 nm);

7. Measurement is performed.

Figure 6 illustrates the band zero adjustment procedure for flat mirrors.

4. Band zero adjustment method for cylindrical mirrors

In contrast to flat mirrors, aspherical (actually any non-flat mirrors) mirrors are always prone to the tracing error effect during measurement relative to the whole reference surface,

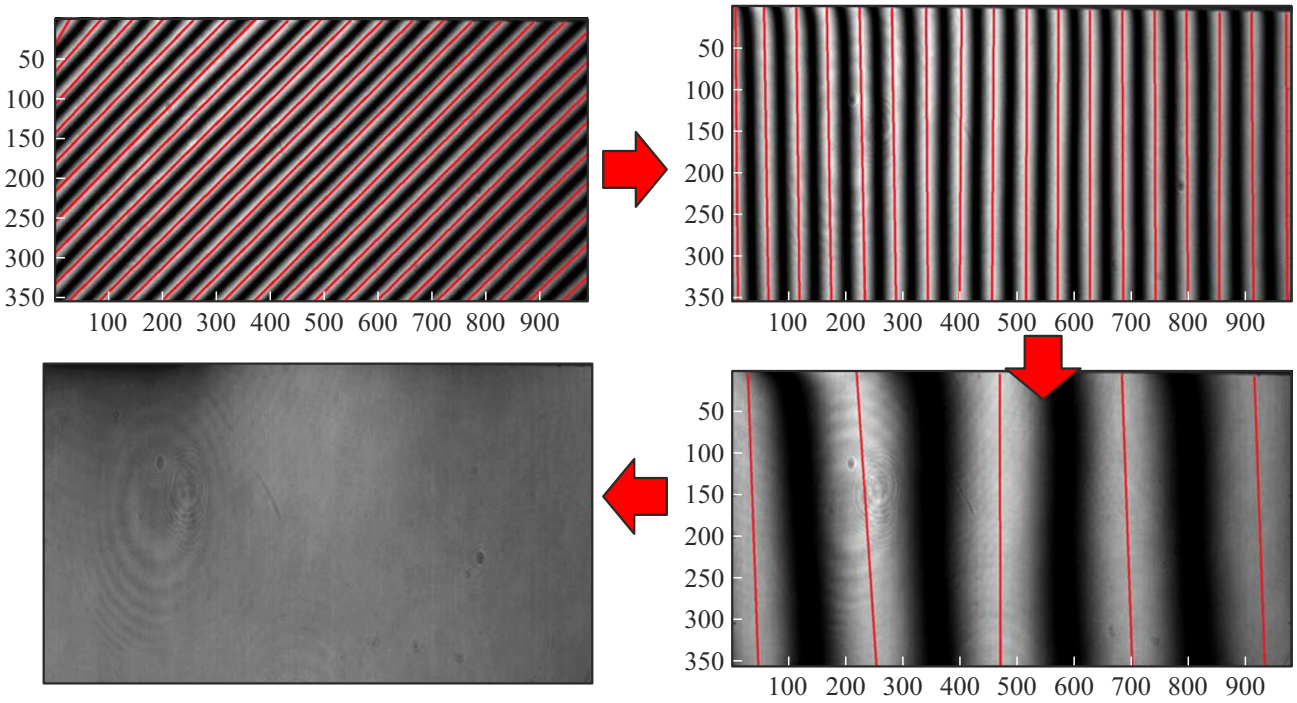

Figure 6. Schematic diagram of band zero adjustment for flat mirrors. Using the rotation stage, the mean angle of slope of approximating straight lines is set to 90°. Then, the ϑY rotation stage is used to reduce the number of bands to one, and the band zero backlash adjustment algorithm is used to achieve an interference pattern with threshold intensity.

and a zero band state cannot be achieved on the whole mirror surface . Therefore, when measuring aspherical mirrors, an interference pattern area with the minimum number of bands shall be selected, and measurements shall be performed in this region.

To minimize the tracing error for aspheric mirrors, the following movement algorithm was developed.

1. Select a region with the lowest density of interference bands (Figure 7), a cylinder interference pattern, on the interference pattern.

2. Binarized image of the interference pattern divides the latter into regions of ones and zeros. Ones correspond to bright bands, and zeros correspond to dark bands. For further reasoning, it is assumed that there are N bright bands;

3. To select white bands for further processing, they are divided into groups. Each white band is checked for a parabolic shape and breaks in the test region.

4. Approximate the selected curves by the parabolic function $y = ax^2 + bx + c$ using the least-square method.

5. Find the minimum coordinate$x = -\frac{b}{2a}$ for the resulting curves. Then, find the mean minimum coordinate and trace it.

6. Use the ϑY translation stage to move the minimum coordinate to the center of the test region.

7. Use the ϑX translation stage to bring the number of parabolas to one.

8. Use the ϑX translation stage to achieve the backlash state with mean interference pattern intensity threshold.

9. Wait for 10 s.

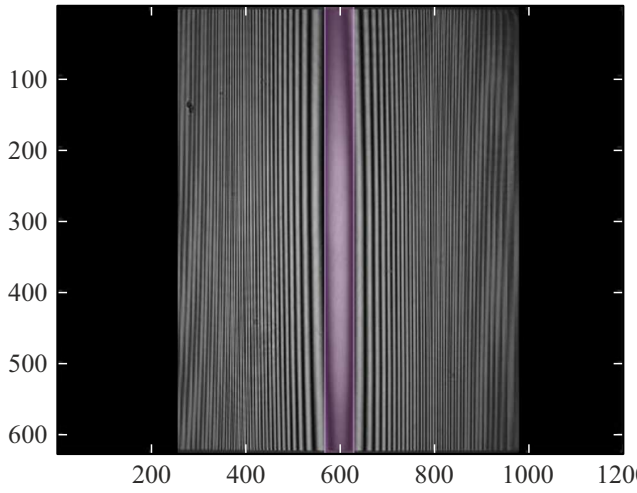

Figure 7. Cylinder interference pattern with the applied mask. The mask highlights a region with „zero bands“, where measurements are least of all prone to the tracing error.

10. Perform the measurement.

Figure 8 illustrates the zero band adjustment procedure for cylindrical mirrors.

5. Improvement of contrast on silicon

For latest-generation synchrotrons, mirrors are generally made from single crystal silicon [28]. Our interferometer uses a fused silica reference surface to obtain high-contrast

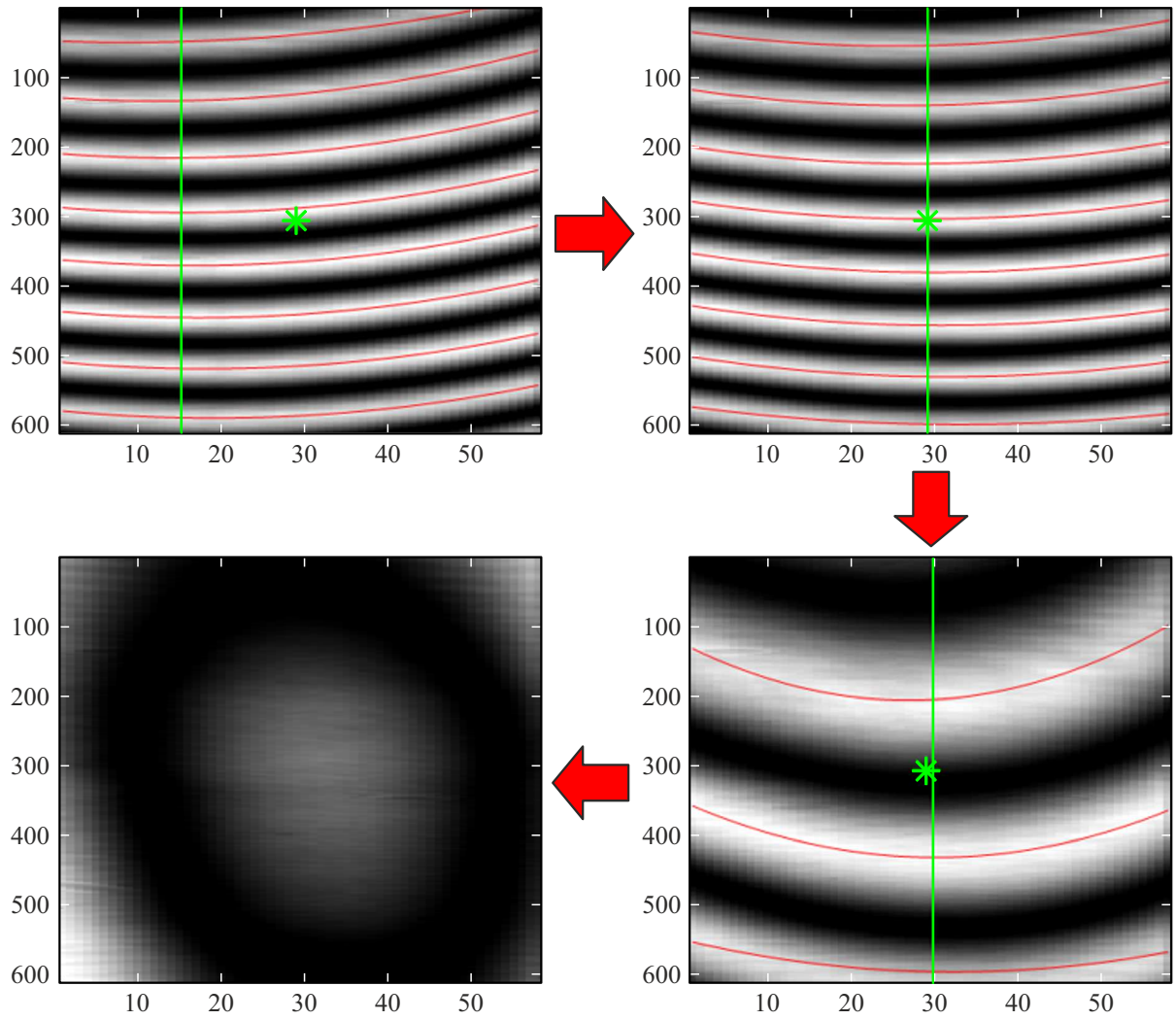

Figure 8. Schematic diagram of zero band adjustment for cylindrical mirrors. Arrows show the path from the initial to the final interference pattern. Red curves show parabolas approximating white interference bands that are used for feedback. A green vertical line corresponds to the mean x-coordinate of parabola vertices. Green asterisk shows the center of the image, to which the vertical line tends. When the line have been aligned with the center, the number of parabolas is minimized and the mean interference pattern intensity threshold is reached for backlashes.

interference patterns from quartz substrates. Binarization threshold in zero band adjustment algorithms is determined using the Otsu method [29] that provides good results during binarization of the interference pattern obtained on quartz. Interference patterns recorded on silicon substrates have a lower contrast due to the difference between coefficients of laser light reflection from fused silica (reference surface material) and silicon, which, together with nonuniform distribution of the reference wavefront intensity induced by damaged reference surface coating on the CMOS matrix of the interferometer detector, becomes a reason why bright interference bands become dark during binarization.

To process interference patterns recorded on silicon, an adaptive histogram equalization method with contrast limitation was selected experimentally [30]. Figure 9 shows that this method provides resolution of all interference bands.

6. Main measurement methods using the created system

The created system provides effective measurements using flat and cylindrical mirror cross-linking techniques and measurement bias determination using the shift method.

For flat mirror measurement using the cross-linking technique, a rectangular digital mask is defined on the aperture for subaperture measurements. The maximum possible mask size is selected, however, the mask shall not cover the reference surface edges to avoid edge effects. Then, the mirror length and cross-linking pitch are programmed so that the overlap area between two successive subapertures

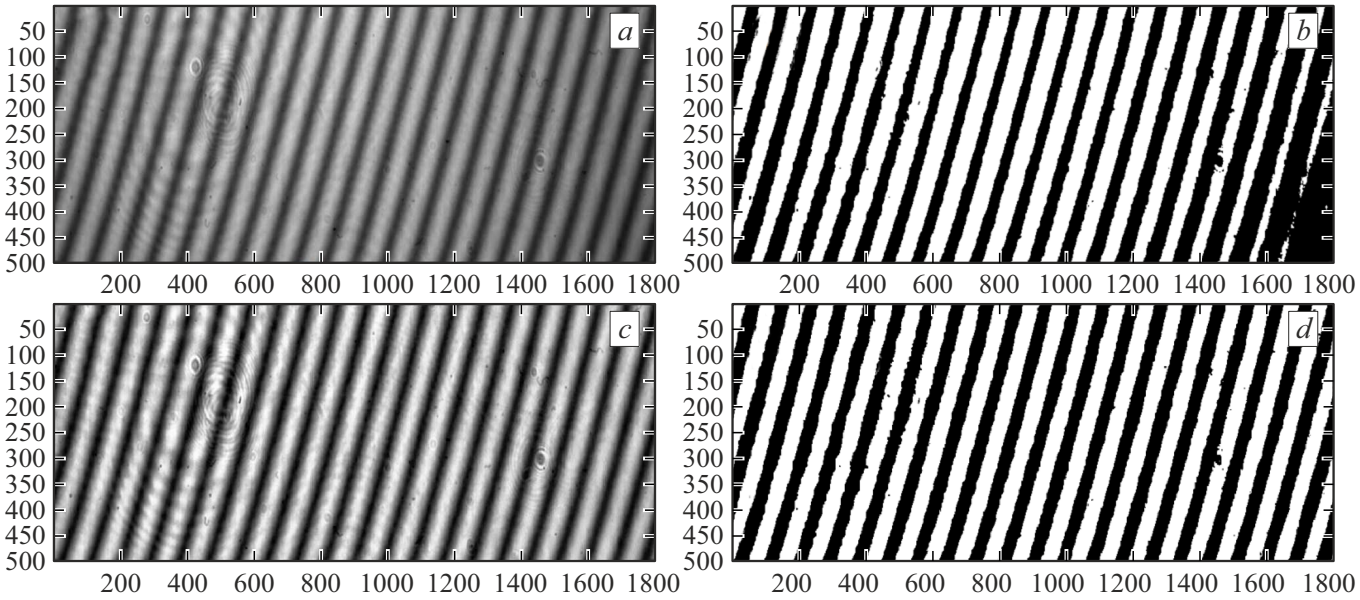

Figure 9. Improvement of contrast on silicon using the adaptive histogram equalization method: *a* — interference pattern before contrast improvement; *b* — binarized image (*a*); *c* — interference pattern after contrast improvement; *d* — binarized image (*c*).

is at least 90% (a globally recognized value) of the mask size [31]. Then,the ϑX and ϑZ translation stages are used to set zero bands for flat mirrors. Then wait for 10 s, believing that the mirror will reach the mechanical equilibrium state. To reduce the random error effect, the measurement is carried out with averaging over 20 frames. After the measurement with the Z translation stage, mirror indexing is performed using the cross-linking pitch and the ϑY translation stage is used to set a large number of bands to trace the band angle variation with better resolution in single-step scanning mode. At the end of measurements, subaperture images are crosslinked using the overlap matrix method [9].

When measuring cylindrical mirrors, the tracing error cannot be generally avoided throughout the visible interferometer aperture. Therefore, the mask size is selected so that it contains the minimum number of interference bands (Figure 7). The next steps are similar to flat mirror cross-linking technique.

The shift method is an effective bias determination method [14,15]. The movement algorithm for this method is similar to that for the flat mirror subaperture cross-linking method. Compared with the three plane method, it allows for prompt bias consideration during mirror measurement by the cross-linking method. This is particularly important for measurement systems that are used in variable climatic conditions, because the medium refractive index, reference and test surface shapes depend on temperature [24] and the reference surface shape depends on humidity [32].

Figure 10 shows the measurements of a cylindrical ellipse and 200 mm long plane using the subaperture cross-linking technique. As shown from Figure 10, the developed techniques can be used to measure cylindrical surfaces with maximum out-of-plane deviation equal to tens of μm on an interferometer with a flat reference wavefront. Figure 11 shows the result of measurement bias consideration in the 20×40 mm reference surface area using a flat mirror. The measured RMSD of the reference surface fragment was about 1.09 nm, and the RMSD of the mirror fragment was 0.62 nm, which indicates that subnanometer accuracy measurements may be performed using the created measurement system.

Conclusion

The main findings are as follows.

1. Institute of Physics of Microstructures, Russian Academy of Sciences, has created an automated 3*D* system on the basis of the Zygo Verifire Fizeau interferometer with a flat reference surface for measuring large flat and cylindrical mirrors, including parabolic and elliptical cylindrical mirrors.

2. For the system, an algorithm was developed to provide automatic sample orientation parallel to the interferometer reference surface in the test region. The algorithm is applicable to flat and cylindrical mirrors.

3. The developed zero band adjustment algorithm minimizes the tracing error. The tracing error in our measurements is less than 1 nm with respect to RMSD.

4. The vibration protection system, ambient air protection system and algorithm adaptation for stepper motors without using the holding mode provide a measurement repeatability of 15 pm.

5. The created system provides effective measurements of large flat and cylindrical mirrors using the subaperture cross-

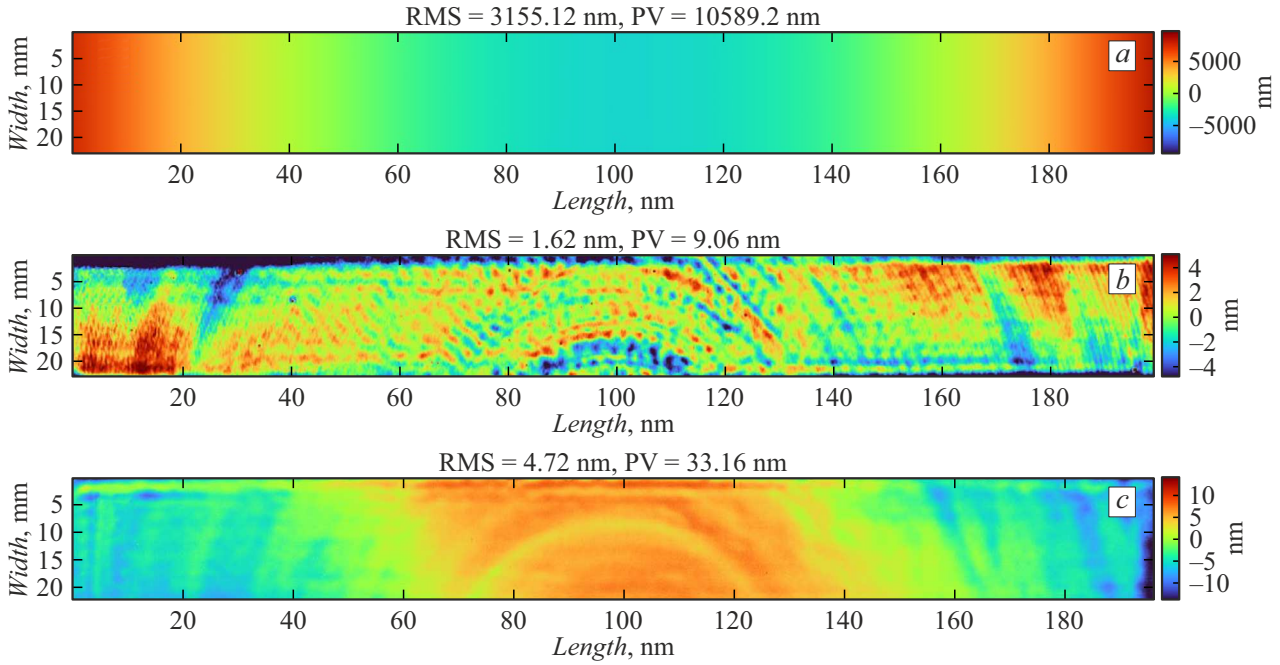

Figure 10. *a* — result of cross-linking of 200 subaperture of an elliptical cylindrical mirror; *b* — deviation of the crosslinked shape from the nearest elliptical cylinder; *c* — result of crosslinking of 200 subapertures of a flat mirror.

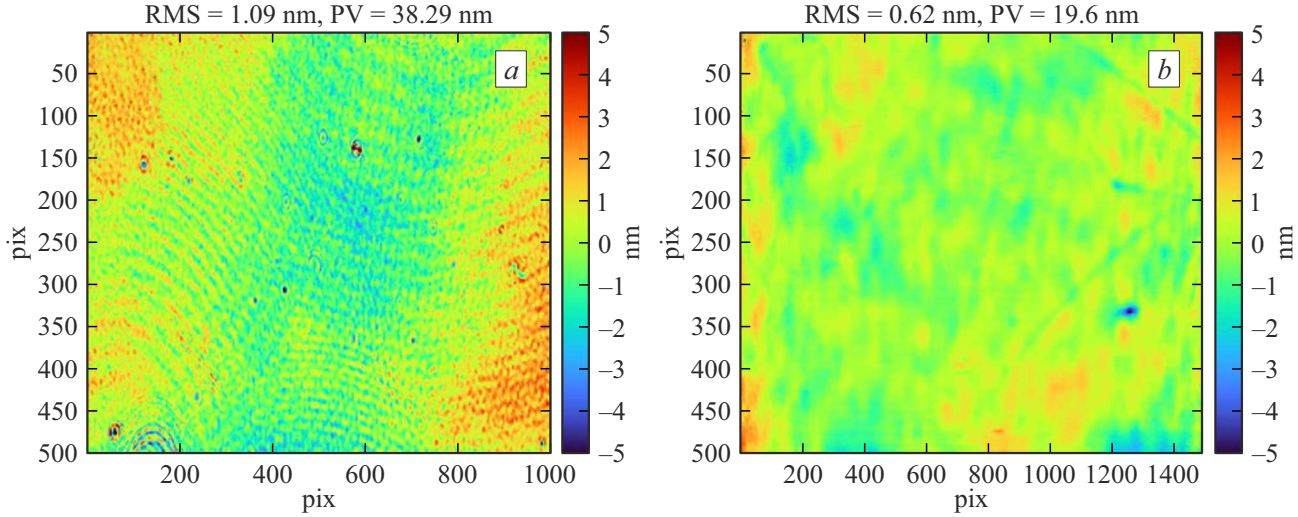

Figure 11. Experimental result for measurement bias determination using the shift method, 1 pixel is equal to 40 μm: *a* — bias; *b* — test mirror.

linking technique, and measurement bias determination using the shift method.

Funding

The study was supported by grant of the Russian Science Foundation № 21-72-30029-P.

Conflict of interest

The authors declare that they have no conflict of interest.

References

[1] Y. Wang, F. Xie, S. Ma, L. Dong. Opt. Lasers Engin., **93**, 164 (2017). DOI: 10.1016/j.optlaseng.2017.02.004

[2] A. Vivo, B. Lantelme, R. Baker, R. Barrett. Rev. Sci. Instrum., **87** (5), 051908 (2016). DOI: 10.1063/1.4950745

[3] M. Bray. SPIE, **3739**, 259 (1999). DOI: 10.1117/12.360153

[4] A. Rommeveaux, M. Thomasset, D. Cocco. In: *Modern Developments in X-ray and Neutron Optics* (Berlin, Heidelberg: Springer Berlin Heidelberg, 2008), p. 181–191. DOI: 10.1007/978-3-540-74561-7_10

[5] F. Siewert, T. Noll, T. Schlegel, T. Zeschke, H. Lammert. AIP Conf. Proceed., **705** (1), 847 (2004). DOI: 10.1063/1.1757928
[6] Y. Shi, X. Xu, Q. Huang, H. Wang, A. Li, L. Zhang, Z. Wang. SPIE, **10385**, 143 (2017). DOI: 10.1117/12.2273793
[7] L. Huang, J. Xue, B. Gao, M. Idir. Opt. Express, **26** (8), 9882 (2018). DOI: 10.1364/oe.26.009882
[8] H. Yumoto, T. Koyama, S. Matsuyama, K. Yamauchi, H. Ohashi. Rev. Sci. Instrum., **87** (5), 051905 (2016). DOI: 10.1063/1.4950714
[9] M. Otsubo, K. Okada, J. Tsujiuchi. Opt. Engineer., **33** (2), 608 (1994). DOI: https://doi.org/10.1117/12.152248
[10] I. Powell, E. Goulet. Appl. Optics, **37** (13), 2579 (1998). DOI: 10.1364/AO.37.002579
[11] P.B. Keenan. SPIE, **429**, 2 (1983). DOI: 10.1117/12.936333
[12] B.S. Fritz. Opt. Engineer., **23** (4), 379 (1984). DOI: 10.1117/12.7973304
[13] A. Kochetkov, A. Shaykin, I. Yakovlev, E. Khazanov, A. Cheplakov, B. Wang, Y. Jin, S. Liu, J. Shao. Opt. Express, **33** (6), 13673 (2025). DOI: 10.1364/OE.551097
[14] G. Zhou, J. Wang, W. Lei, X. Dong, J. Wang. Appl. Optics, **63** (8), 2086 (2024). DOI: 10.1364/AO.516190
[15] Z. Guang, L. Weizheng, D. Xiaohao, W. Jie. Laser Optoelectron. Progress, **60** (23), 2312001 (2023). DOI: 10.3788/LOP222992
[16] E.V. Petrakov, N.I. Chkhalo, A.K. Chernyshev, E.I. Glushkov. Opt. Engineer., **63** (11), 114104-1 (2024). DOI: 10.1117/1.OE.63.11.114104
[17] Ya.V. Zubavichus. *Tekhnologicheskaya infrastruktura sibirskogo kol'tsevogo istichnika fotonov „SKIF“. T. 1. Eksperimentalnye stantsii pervoi ocheredi i Laboratorny kompleks* (In-t kataliza im. G.K. Boreskova SO RAN, Novosibirsk, 2022) (in Russian)
[18] Ya.V. Rakshun, Yu.V. Khomyakov, E.I. Glushkov, A.S. Gogolev, M.V. Gorbachev, A.V. Dar'in, F.A. Dar'in, I.P. Dolbnya, S.V. Rashchenko, V.A. Tchernov, N.I. Chkhalo, M.R. Sharafutdinov. Izvestiya TPU. Inzhiniring georesursov, **336** (5), 229 (2025).(in Russian) DOI: 10.18799/24131830/2025/5/5122
[19] V.A. Chernov, I.A. Bataev, Y.V. Rakshun, Y.V. Khomyakov, M.V. Gorbachev, A.E. Trebushinin, N.I. Chkhalo, D.A. Krasnorutskiy, V.S. Naumkin, A.N. Sklyarov, N.A. Mezentsev, A.M. Korsunsky, I.P. Dolbnya. Rev. Sci. Instrum., **94** (1), 013305 (2023). DOI: 10.1063/5.0103481
[20] S.V. Rashchenko, M.A. Skamarokha, G.N. Baranov, Y.V. Zubavichus, I.V. Rakshun. AIP Conf. Proceed., **2299** (1), 060001 (2020). DOI: 10.1063/5.0030346
[21] N.I. Chkhalo, S.A. Garakhin, I.V. Malyshev, V.N. Polkovnikov, M.N. Toropov, N.N. Salashchenko, B.A. Ulasevich, Ya.V. Rakshun, V.A. Chernov, I.P. Dolbnya, S.V. Raschenko. ZhTF, **92** (8), 1261 (2022) (in Russian). DOI: 10.21883/JTF.2022.08.52794.100-22
[22] E.I. Glushkov, I.V. Malyshev, E.V. Petrakov, N.I. Chkhalo, Yu.V. Khomyakov, Ya.V. Rakshun, V.A. Chernov, I.P. Dolbnya. J. Surf. Investig., **17** (1), S233 (2023). DOI: 10.1134/S1027451023070133
[23] Electronic source. Available at: https://www.standa.lt/
[24] M. Erlong, G. Yongqiang. Acta Optica Sinica, **31** (12), 1212008 (2011). DOI: 10.3788/aos201131.1212008
[25] A. Vivo, R. Barrett. SPIE, **10385**, 149 (2017). DOI: 10.1117/12.2274745
[26] P. de Groot. Appl. Opt., **44** (33), 7062 (2005). DOI: 10.1364/AO.44.007062
[27] C.B. Kreischer. SPIE, **8884**, 189 (2013). DOI: 10.1117/12.2029324
[28] A. Erko, M. Idir, T. Krist, A. Michette. In: *Modern developments in X-ray and neutron optics*, **137** (Springer, Berlin, 2008), DOI: 10.1007/978-3-540-74561-7
[29] N. Otsu. IEEE Transactions on Systems, Man, and Cybernetics, **9** (1), 62 (1979). DOI: 10.1109/TSMC.1979.4310076
[30] K. Zuiderveld. *Graphic Gems. Contrast Limited Adaptive Histogram Equalization* (Academic Press Professional, San Diego, 1994), p. 474–485. DOI: 10.1016/B978-0-12-336156-1.50061-6
[31] M.B. Da Silva, S.G. Alcock, I.T. Nistea, K. Sawhney. Opt. Lasers in Engineer., **161**, 107192 (2023). DOI: 10.1016/j.optlaseng.2022.107192
[32] H. Yumoto, S. Matsuyama, H. Mimura, K. Yamauchi, H. Ohashi. Nuclear Instruments and Methods in Physics Research Section A: Accelerators, Spectrometers, Detectors and Associated Equipment, **710**, 2 (2013). DOI: 10.1016/j.nima.2012.10.126

Translated by E.Ilinskaya